Estimation of Local Equilibrium Foam Model Parameters as Functions of the Foam Quality and the Total Superficial Velocity

Alexandre Vicard,* Olivier Atteia,* Henri Bertin, and Jean Lachaud
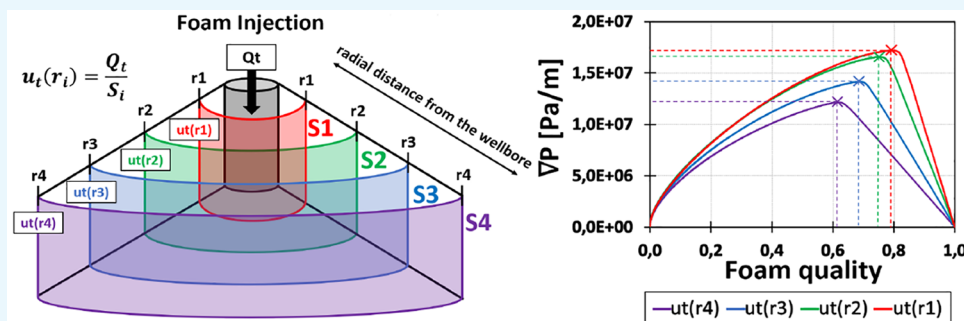
Read Online

ACCESS | Metrics & More | Article Recommendations | Supporting Information

ABSTRACT: In this paper, the behavior of foam in a porous medium is studied in order to understand the effect of the fluid velocity on foam properties. This aspect is crucial during foam injection, as due to radial effects the foam velocity largely decreases around the injection well. The foam properties are detailed through the use of a new local equilibrium foam model parameter estimation approach using an improved new shear function and based on the most widely used STARS model developed by the Computer Modeling Group (CMG). A new mode of calculation of the STARS model parameters is then presented in order to allow both a semiautomated fitting of several quality scan pressure curves and a consideration of the role of the total velocity. The approach is tested through column experiments done at various velocities and gas fractions. Furthermore, the proposed model is also tested on literature results in order to validate it for very different experimental conditions. This study and the fitted results are then used to understand, on both our column experiments and the literature data, the existence of two shear effects and their origins.

INTRODUCTION

Foam injection in porous media was commonly used with several objectives such as diversion of acid or gas for improved oil recovery (IOR)[1−3] and mobilization or solubilization of contaminants for in situ environmental remediation (ISER).[4−6]

Foam in porous media is formed by gas bubbles separated by liquid films called lamellae. Foam behavior is inherently linked to the porous media characteristics (pore size, distribution, etc.) through a creation and destruction dynamic of lamellae.[7] These lamellae are in situ generated throughout snap-off, lamellae division and are left behind when they collapse due to gravity drainage, gas diffusion, and capillary suction.[8] Foam could be stabilized by amphiphilic molecules called surfactants, which reduced the interfacial tension at the bubble gas−liquid interface (i.e., lamellae). Therefore, lamellae dynamics and displacement create a resistance to the gas flow, which reduces gas relative permeability (i.e., mobility) and increases the apparent viscosity of the foam that diverts flow from large pores to smaller ones.

Several experiments demonstrated that foam flow in porous media is composed of two distinct regimes, the high and the low quality regimes.[9,10] The foam quality represents the gas fraction in the liquid/gas mixture, which is injected. On one hand, in the low quality regime when the foam quality increases, the pressure gradient or apparent viscosity of the foam increases. In this regime, bubble trapping and mobilization dominate the foam flow with a possible shear thinning effect. On the other hand, in the high quality regime when the foam quality increases, the pressure gradient or the apparent viscosity of the foam decreases. In this regime gas bubbles are separated by thin lamellae, which are unstable, and the flow is dominated by lamellae breaks and the concept of limiting capillary pressure P_c^*.[11]

Foam models are usually divided into two groups, the population balanced (PB) model and local equilibrium (LE) model. The explicit PB models describe lamellae generation and destruction happening at the pore scale. This type of model is generally not viable for large scale simulation due to

its expensive computational cost and its number of parameters. This is why LE models are widely used for large scale reservoir simulation thanks to their implicit approach, which consists of a single empirical formula to control the gas phase mobility. Thus, it could be easily integrated to a two phase flow generalized Darcy model using relative permeability models.[12,13] Parameters of the LE model are estimated from foam flooding experiment data through different kinds of methods[14−16] during a steady state foam flow. One of the most commonly used LE foam models, named STARS, comes from the Computing Modeling Group (CMG). This model approaches foam behavior by modifying the gas relative permeability with a "mobility factor" (FM). The FM factor can be calculated as a function of several variables where each of them expresses a particular foam behavior. Cheng et al.[15] give a detailed description of these variables that can compose the FM function.

For ISER applications, the radial effect needs to be considered to qualify the foam behavior as the foam is injected in a wellbore. For this purpose, numerical simulations with an LE foam model are generally used. Although the foam behavior has been shown to vary with the total superficial velocity,[9,10,17] to our knowledge no studies considered STARS model parameters varying with the distance from the well. This is the major objective of this paper, where the foam parameters are modeled for the whole range of quality scans including u_t variations. In order to do so, a reformulation of the shear effect was necessary to take under consideration both the role of the foam quality and u_t on the whole quality scan. This new approach was supported by new 1-D foam flooding experiments and was then extended to other experiments available in the literature. The link between the parameters and u_t allowed us then to expand the approach to the study of radial effects during foam injection.

FOAM MODEL

STARS Foam Model. STARS, from the Computing Modeling Group (CMG), is a commercial reservoir simulator including a texture-implicit local equilibrium (LE) foam model. In this model, the foam behavior is introduced by multiplying the gas relative permeability k_{rg} by a mobility reduction factor FM. Thus, a new foam equivalent relative permeability k_{rg}^f is obtained. The factor FM is presented within the generalized Darcy expression of the gaseous phase in eq 1.

$$u_f f_g = -\frac{k k_{rg}^f}{\mu_g}(\nabla P_g - \rho_g g) \quad \text{with} \quad k_{rg}^f = k_{rg} \times \text{FM} \tag{1}$$

where u_t is the total superficial velocity ($u_t = u_g + u_w$), f_g the foam quality with $f_g = \frac{u_g}{u_t}$, k the intrinsic permeability, k_{rg} the relative permeability of the gas phase without foam, and μ_g the gas dynamic viscosity. The gas pressure gradient ∇P_g and water pressure gradient ∇P_w are linked through the capillary pressure expression $P_c(S_w) = P_g - P_w$. Furthermore, if 1-D experiments are conducted horizontally, the gravitational contribution for each phase can be neglected during the foam model parameter estimation process.

FM is dimensionless and composed of a given number of dimensionless subfunctions shown in eq 2. These subfunctions describe the foam behavior against a given factor such as water saturation, surfactant concentration, oil saturation, non-Newtonian behavior, foam generation, salinity, etc.

$$\text{FM} = \frac{1}{1 + fmmob \times \prod_{i=1}^{n} F_i} \tag{2}$$

The parameter $fmmob$ represents the highest mobility reduction factor reachable for wet foam. F_i subfunctions are defined within the range ($0 \leq F_i \leq 1$). From this definition the foam at a given quality f_g and total superficial velocity u_t obtains its maximum gas mobility reduction when all F_i subfunctions are equal to 1. In this paper two subfunctions are considered, the water saturation dependence or dry out subfunction F_{dry} and the shear rate dependence subfunction F_{shear}. Then, eq 2 is reduced to

$$\text{FM} = \frac{1}{1 + fmmob \times F_{dry} \times F_{shear}} \tag{3}$$

F_{dry} is the water saturation dependence subfunction which is continuous and increases with S_w as presented in eq 4.

$$F_{dry} = 0.5 + \frac{\arctan(epdry(S_w - fmdry))}{\pi} \tag{4}$$

F_{dry} contains two parameters: $fmdry$ and $epdry$. $fmdry$ is defined as the critical water saturation under which foam collapses and is often confused with S_w^*, the water saturation at the transition point where the foam strength is maximal. S_w^* is often linked to the limiting capillary pressure P_c^* in the literature,[15,18] the pressure above which the capillary pressure dries out lamellae and leads to their rupture. $epdry$ controls the abruptness of the foam collapse. A large value of $epdry$ implies a sharp dry out of the foam as soon as the water saturation approaches the S_w^* value. Due to the sharp pressure gradient decrease at this point, S_w^* and $fmdry$ values are very close and could be confused. The role of $epdry$ on the distinction between $fmdry$ and S_w^* and how $epdry$ can be used to calculate $fmdry$ from S_w^* are presented within the Fitting Method section.

F_{shear} (also called F_{cap}) is the shear rate dependence subfunction using the local capillary number N_{Ca} as presented in eq 5.

$$\text{if } N_{ca} > fmcap, F_{shear} = \left(\frac{fmcap}{N_{Ca}}\right)^{epcap}; \text{ otherwise, } F_{shear} = 1 \tag{5}$$

The parameter $epcap$ controls how foam rheology is dependent on the shear rate. A positive value of $epcap$ corresponds to a shear-thinning behavior. $fmcap$ is a parameter used to normalized the F_{shear} value within the range $[0, 1]$. N_{Ca} is a dimensionless number in fluid mechanics which compares viscous and capillary forces. A high N_{Ca} value implies higher viscous effects and, thus, a high shear rate. The expression of the capillary number remains controversial in the literature,[9,14,19,20] and its use differs from one to another parameter optimization process; it has been used with two significations.

On one hand, the F_{shear} subfunction is used to modify the value of the maximum apparent viscosity of the foam for different superficial velocities. As an example, in the experiments of Zeng et al.[19] the capillary number N_{Ca} was defined using the total superficial velocity and the surface tension between the gaseous and the aqueous phases. The transition foam quality f_g^* observed on a single quality scan was determined, and several experiments at this f_g^* with various total superficial velocities u_t were performed. It seems that a fixed f_g^* point for all u_t values was assumed. Zeng et al.[19] also
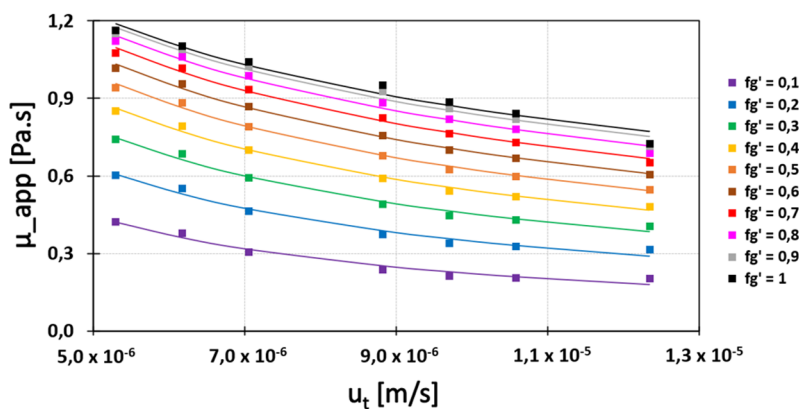
Figure 1. Apparent viscosity μ_{app} plotted against the total superficial velocity u_t from the Alvarez et al. experimental data. Each group of colored squares corresponds to various values of $f'_g = f_g/f^*_g$. In this plot, note that $f'_g = \in [0, 1]$ and that the f'_g increase is constant between each color. Final fits using $K(f'_g)$ and $(n-1)(f'_g)$ functions are also plotted with colored lines to validate eq 8.
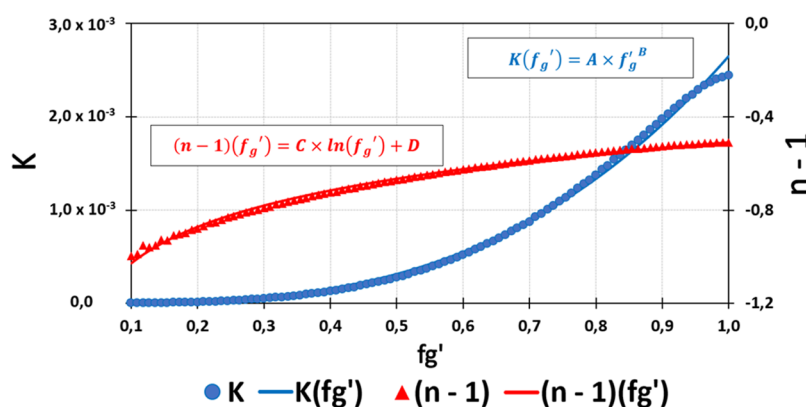
Figure 2. Obtained K and $(n-1)$ values from the first set of the SLSQP plotted against f'_g with blue circles and red triangles, respectively. K and $(n-1)$ functions of f'_g using parameters A, B, C, and D were fitted using a second set of the SLSQP and presented with blue and red lines, respectively. $A = 2.6462 \times 10^{-3}$, $B = 3.0713$, $C = 2.2530 \times 10^{-1}$, and $D = -5.0865 \times 10^{-1}$.

used a very low *epdry* value to obtain a curved shape able to capture experimental points within the low quality regime. This technique would be limited for a case with an abrupt foam collapse. In addition, using a low *epdry* with the assumption that $S^*_w = fmdry$ seems not relevant with regard to the literature.[16]

On the other hand, the F_{shear} subfunction is used to catch experimental points within the low quality regime of the quality scan, which are often underestimated using the subfunction F_{dry} alone.[14,21] The capillary number is defined using the pressure gradient, which requires iterations for convergence. Furthermore, to keep F_{shear} within the range [0, 1], the *fmmob* value is increased from the first value obtained through F_{dry} alone[14] to compensate the F_{shear} modification (see Figure S1 in the Supporting Information).

Modified Foam STARS Model and Assumptions. For ISER applications, foam is injected through wells leading to a fast decrease of the total superficial velocity u_t with the radial distance. In turn, it modifies the foam properties with distance from the injection point.[17] It therefore appears that for real field applications the STARS model parameters must be u_t dependent functions. Because F_{shear} uses a description within FM, we present below an approach which takes u_t variations into account with an improved shear dependence expression. Note that only the low quality regime is studied below ($0 \leq f_g$

$\leq f^*_g$) as the F_{dry} subfunction used to describe the high quality regime (foam collapse) has already been detailed previously.

In their paper, Alvarez et al.[9] provide numerous experimental results of foam injections with pressure contour plots. These data show a foam quality value at the transition f^*_g increasing with u_t, which was never taken into account within LE foam models to our knowledge. As the f^*_g value is a function of u_t in this case with $f^*_g(u_t) \in [0.5, 0.9]$, we defined the relative position from the f^*_g point within the low quality regime as $f'_g = f_g/f^*_g$. f'_g is a shared and comparable parameter for all u_t quality scans (various injected foam qualities for a fixed u_t value). f^*_g values were estimated with a correct accuracy thanks to the amount of data for various u_t values close to the transition points. Using the apparent viscosity definition presented eq 6, we plotted $\mu_{app} = f(u_t)$ curves for various values of f'_g within the low quality regime on Figure 1.

$$\mu_{app} = \frac{k \nabla P}{u_t} \tag{6}$$

Colored squares on Figure 1 show that there is a dependency of μ_{app} both on u_t and on f'_g. In fact, μ_{app} is a nonlinear function of u_t with coefficients changing with f'_g. This led us to consider the curves $\mu_{app} = f(u_t)|_{f'_g}$ for various fixed f'_g values. We opted for an Ostwald−de Waele type law using the total superficial velocity u_t presented hereafter:
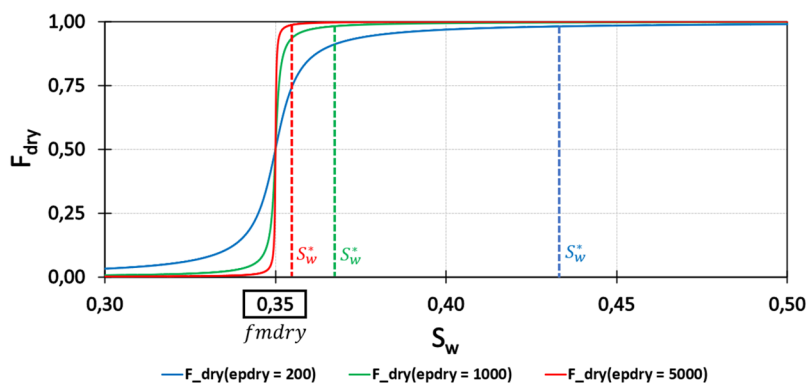
Figure 3. F_{shear} plotted against S_w for *epdry* = [200, 1000, 5000] with blue, green, and red curves, respectively. *fmdry* was set to 0.35 for the example and is indicated with a black rectangle on the S_w axis. Estimated S_w^* values are given using colored dotted straight lines for the three different *epdry* values.

$$\mu_{app} = K \times u_t^{(n-1)} \tag{7}$$

with K the consistency factor and $(n-1)$ the flow behavior exponent. The classical Ostwald−de Waele law uses the shear rate as $\mu_{app} = K\dot{\gamma}^{n-1}$, and we simplified the relation using the total superficial velocity, which is still a good indicator of the shear rate as the steady state is reached for all experiments. A first set of fits were made using a sequential least-squares program (SLSQP). We present on Figure 2 the obtained K and $(n-1)$ values plotted against f_g for all velocities with blue circles and red triangles, respectively.

Using the obtained K and $(n-1)$ shapes against f_g, two functions $K(f_g')$ and $(n-1)(f_g')$ were set and are presented in Figure 2. The expression of the apparent viscosity as a function of f_g' and u_t is presented below:

$$\mu_{app} = A \times (f_g')^B \times u_t^{C\times \ln(f_g')+D} \tag{8}$$

with A, B, C, and D the determined constants of K and $(n-1)$ functions of f_g'. A second set of the SLSQP were done to determine A, B, C, and D values (see Figure 2). $K(f_g')$ and $(n-1)(f_g')$ fitted curves are given Figure 2 with blue and red lines, respectively. Equation 8 fit accurately the original experimental data set, providing the expected apparent viscosity variations as presented Figure 1 with colored lines. It is clear, however, that these expressions are not constants as has been used up to present. In this formulation, K and $(n-1)$ depend on foam quality, which has not been shown previously to our knowledge.

Fitting Method Using F_{dry} and the New Function F_{shear}. In this section we present a fitting method to determine F_{dry} (eq 4) and F_{shear} (eq 13) parameters, and this method needs several quality scans ($\nabla P(f_g)$ curves for various u_t values). It appeared from several optimization processes that the D parameter used for the F_{shear} subfunction was not essential for the fit. Thus, D was set to zero by default to decrease the number of parameters within F_{shear}. For the fitting process, the generalized Darcy equations for gas, eq 9, and water, eq 10, are simplified to the following expressions without capillary pressure nor gravity effects:

$$u_t f_g = k\lambda_{rg}FM\nabla P \quad \text{with } \lambda_{rg} = \frac{k_{rg}}{\mu_g} \tag{9}$$

$$u_t(1-f_g) = k\lambda_{rw}\nabla P \quad \text{with } \lambda_{rw} = \frac{k_{rw}}{\mu_w} \tag{10}$$

Note here that for simplification we use the absolute value of the pressure gradient ∇P. λ_{rg} and λ_{rw} are the gas and water mobilities, respectively. We used the Brooks and Corey[12] relative permeability model for the two phases. As shown in eq 11 and eq 12, k_{rg}^0 and k_{rw}^0 are the end point relative permeabilities for gas and water, respectively, $S_{g,r}$ is the gas residual saturation, $S_{w,r}$ is the water residual saturation, and n_g and n_w are the Brooks and Corey model exponents for gas and water, respectively.

$$k_{rg} = k_{rg}^0 \times (1-Se)^{n_g} \quad \text{with Se} = \frac{S_w - S_{w,r}}{1 - S_{w,r} - S_{g,r}} \tag{11}$$

$$k_{rw} = k_{rw}^0 \times (Se)^{n_w} \tag{12}$$

Equations 9 and 10 and the relation $f_g = \frac{u_g}{u_g + u_w}$ were used to express f_g (eq 14) and ∇P (eq 15). In order to do so, and for consistency with eq 14 and eq 15, the F_{shear} subfunction is expressed with S_e and not f_g:

$$F_{shear} = A \times (S_e')^B \times u_t^{C\times \ln(S_e')} \quad \text{with } S_e' = \frac{1-Se}{1-Se*} \tag{13}$$

$$f_g = \frac{\lambda_{rg}FM}{\lambda_{rg}FM + \lambda_{rw}} \tag{14}$$

$$\nabla P = \frac{u_t f_g}{k\lambda_{rg}FM} \tag{15}$$

The fit is done in several steps, as a direct fit does not converge. Five parameters must be optimized to fit the model: f_g^*, ∇P^*, A, B, and C. We assume that *epdry* is constant, and we use it as an input set by the user. This parameter can influence the curvature within the low quality and, thus, interfere with F_{shear} parameters A, B, and C optimization. As a consequence, a few order of magnitude of *epdry* must be tested to find the best one; however, the sharpness of the transition point indicates the order of magnitude of *epdry*. At first a simple polyfit method around the transition point is done using experimental values to provide $(f_g^*, \nabla P^*)$ input values and A, B, and C were set to 1. Then, several optimization steps were done through

python scripts using the scipy.optimize.fmin_slsqp method (sequential least squares programming) on a shared routine presented in Figure S2 in the Supporting Information.

The S_w^* values are obtained through the eq 16 using eq 10 and eq 12

$$S_w^* = \left(\frac{u_t(1 - f_g^*)\mu_w}{k_{rw}^0 k \nabla P^*} \right)^{1/n_w} \times (1 - S_{g,r} - S_{w,r}) + S_{w,r}$$

(16)

During the parameter optimization processes observed in the literature the *fmdry* estimation and distinction from S_w^* is not always clear. In fact the *fmdry* value corresponds to the S_w value at which $F_{dry} = 0.5$ and the S_w^* value corresponds to the transition point, where the pressure gradient is maximal. These two values may be very close for large *epdry* values, but the signification of a large value is left to user appreciation. This is why, as S_w^* is known from eq 16, a method to calculate *fmdry* is defined below.

We present in Figure 3 a plot of F_{dry} against S_w for a fixed *fmdry* and various *epdry* values. For this plot, we considered that the S_w^* value is obtained for $F_{dry} = 0.995$, which corresponds to the beginning of the foam collapse very close to the transition point (0.5% error). Based on these assumptions, we defined the distance between S_w^* and *fmdry* as $\delta S_w = S_w^* - fmdry$, which was calculated as follows using eq 4:

$$\delta S_w = \frac{\alpha}{epdry} \quad \text{with } \alpha = \tan(\pi \times 0.495)$$

(17)

This equation thus allows *fmdry* to be estimated after S_w^* calculation, assuming *epdry* is known. Equation 17 provides an accurate *fmdry* value for *epdry* values above or equal to 200.

The parameter *fmmob* is calculated at the transition point ($f_g = f_g^*$ and $\nabla P = \nabla P^*$) using the eq 19 with the assumption that $F_{dry} = 1$ at the transition and $F_{shear} = A$ at this point.

$$fmdry = S_w^* - \frac{\alpha}{epdry}$$

(18)

$$fmmob = \frac{\left(\frac{k\lambda_{rg} \nabla P}{u_t f_g} - 1 \right)}{F_{dry} F_{shear}}$$

(19)

Then, it is possible to solve eq 14 and eq 15 using S_w variations within the interval $[S_{w,r}, 1 - S_{w,r}]$. A detailed flowchart of the optimization process is given in Figure S2 in the Supporting Information.

■ RESULTS AND DISCUSSION

We will first demonstrate our fitting method results using experiments presented in this paper and two other experimental data sets from the literature. Then, we will discuss our new F_{shear} subfunction integration to the STARS foam model and the radial effect consequences on a field foam injection for ISER application.

Experimental and Parameters Fitting Results. *Saponin Column Results.* We applied the previous fitting method with f_g^* and ∇P^* parameters as u_t functions using data from experiments presented in this paper. Numerical values obtained from the experiments are provided in Table 1. For these experiments, saponin, an environmentally friendly surfactant, has been used with foam pregeneration.

Table 1. Summary of the Flooding Experiments Presented in This Paper

| column no.	k [m^2]	u_t [m/s]	∇P [Pa/m]
C_1	6.97×10^{-11}	1.3393×10^{-4}	3.0944×10^5
($f_g = 0.3$)	-	1.0881×10^{-4}	2.5439×10^5
	-	8.3704×10^{-5}	2.0795×10^5
	-	5.8592×10^{-5}	1.3671×10^5
C_2	3.29×10^{-11}	1.3393×10^{-4}	5.2251×10^5
($f_g = 0.5$)	-	1.0881×10^{-4}	3.9888×10^5
	-	8.3704×10^{-5}	2.8820×10^5
	-	5.8592×10^{-5}	1.8602×10^5
C_3	6.00×10^{-11}	1.3393×10^{-4}	3.3361×10^5
($f_g = 0.7$)	-	1.0881×10^{-4}	2.5077×10^5
	-	8.3704×10^{-5}	1.8675×10^5
	-	5.8592×10^{-5}	1.2733×10^5
C_4	4.97×10^{-11}	1.3393×10^{-4}	2.0214×10^5
($f_g = 0.8$)	-	1.0881×10^{-4}	1.5549×10^5
	-	8.3704×10^{-5}	1.1578×10^5
	-	5.8592×10^{-5}	7.9358×10^4
C_5	4.97×10^{-11}	1.3393×10^{-4}	1.4297×10^5
($f_g = 0.9$)	-	1.0881×10^{-4}	1.1418×10^5
	-	8.3704×10^{-5}	6.5719×10^4
	-	5.8592×10^{-5}	4.1530×10^4

Experimental data results and data fit to each quality scan are given in Figure 4. These fits use $f_g^*(u_t)$ and $\nabla P^*(u_t)$ fitted curves and the three parameters A, B, and C presented Figure 5.

Quality scan f_g^* values are located around $f_g = 0.5$, and the influence of u_t on this parameter seems to be negligible. This is confirmed by the $f_g^*(u_t)$ plot in Figure 5. Thus, $f_g^*(u_t)$ could be interpreted as a constant in this case. The pressure gradient at the transition ∇P^* is quite linear against u_t within the tested range. The *epdry* value was tested with various orders of magnitude, and *epdry* $= 10^4$ provides the best global fit.

Alvarez et al. Experiments, 2001. We applied our fitting method to the Alvarez et al.[9] data. As Figure 6 shows, the resulting fit are quite good. The model illustrates a significant change of f_g^* with the total interstitial velocity u_t, provided in the different subplots. The pressure gradient ∇P also changes for each velocity, increasing with u_t. The model also clearly shows the linear and rapid decrease of ∇P for high f_g after the collapsing point. On the contrary, thanks to the formulation of F_{shear} presented above, the model captures a clear nonlinear behavior for low quality foam, below f_g^*.

$f_g^*(u_t)$ and $\nabla P^*(u_t)$ fitted curves and the A, B, and C constants are given in Figure 7. They illustrate a different behavior than our previous experiments: all parameters are changing with u_t. The parametric equations used to fit the u_t relationships allow a good fit. It must be noticed that the equation itself is the same as for the previous experiments, only the parameters are changing. The pressure gradient at the transition ∇P^* tends to a plateau for high u_t values.

Osterloh et al. Experiments, 1992. These experiments were done at similar velocities to experiments presented in this paper, in lower permeability unconsolidated sand-packs at high temperatures (Figure 8). Under the given conditions, the curves are quite specific in the sense that the f_g^* values are very high. There are no obvious reasons for these high values, and f_g^* shows only very slight variations with u_t. The pressure gradient also increases slightly with u_t. The high f_g^* may explain why the experimental points are present only in the high range
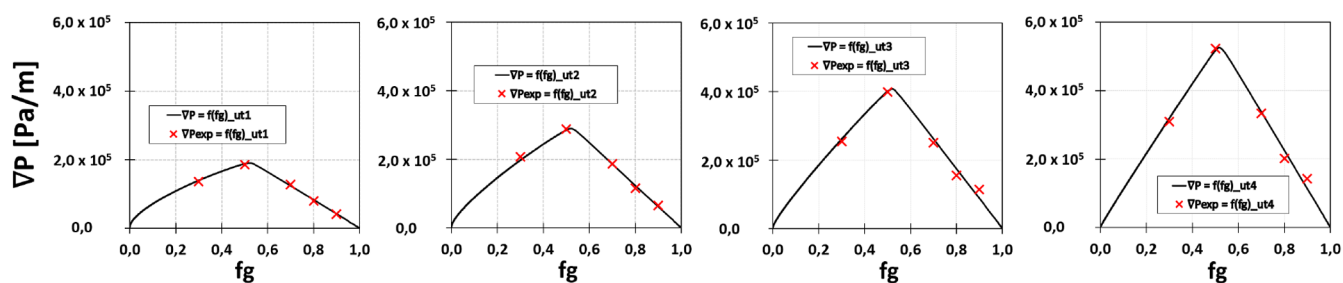
Figure 4. $\nabla P = f(f_g)$ curves fit to experiments presented is this paper. These curves are obtained through parameter functions of u_t and the optimization schema presented Figure S2 in the Supporting Information. *epdry* was set to 10^4 for all u_t values.
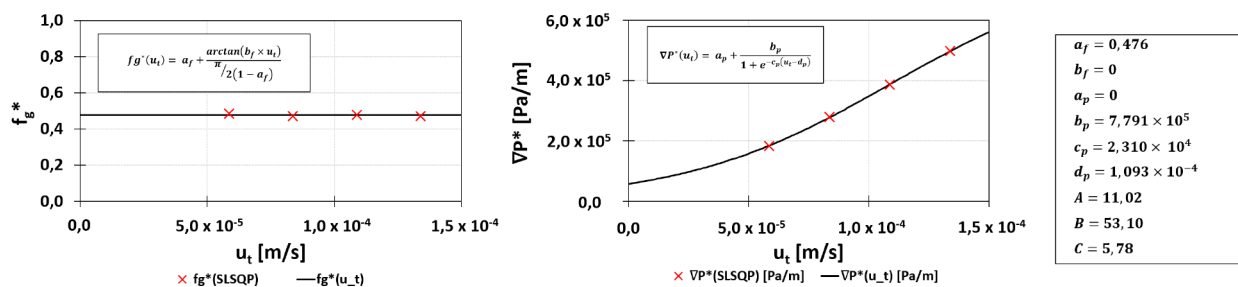
Figure 5. Parameters f_g^* and ∇P^* coming from the optimization process plotted against u_t with their dedicated curve fits and expressions. Red crosses come from the optimization process, and straight black lines represent fitted $f_g^*(u_t)$ and $\nabla P^*(u_t)$ subfunctions. Parameters A, B, and C from the F_{shear} function are also given. This figure gathers all the information needed to cover all foam injection cases within the range of u_t studied.
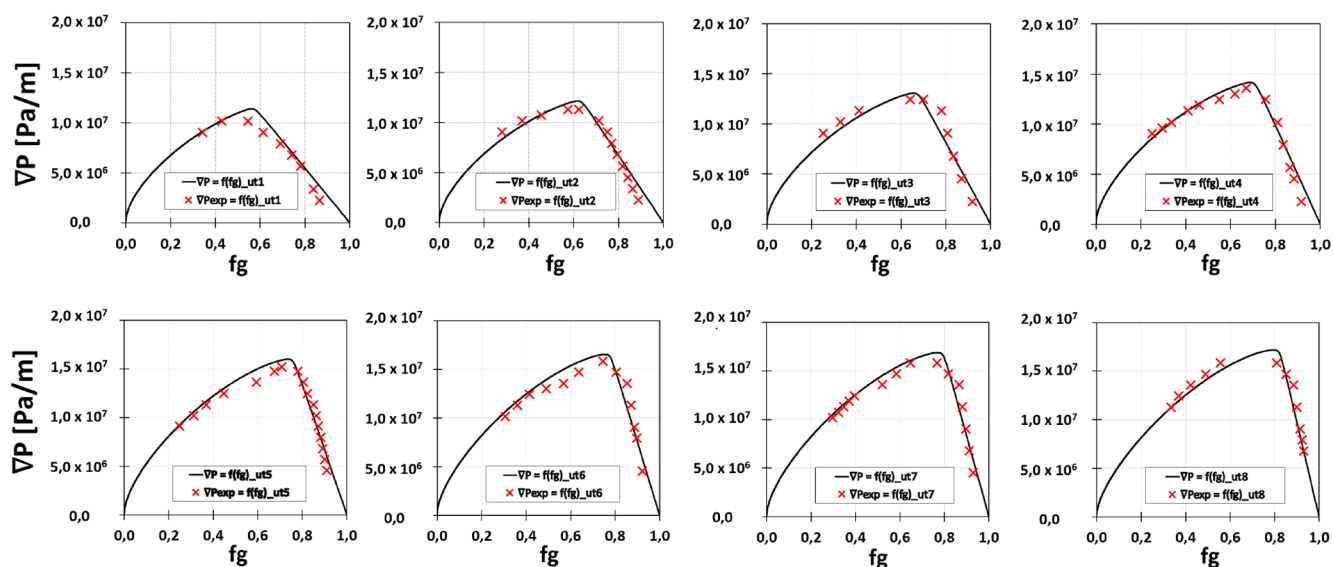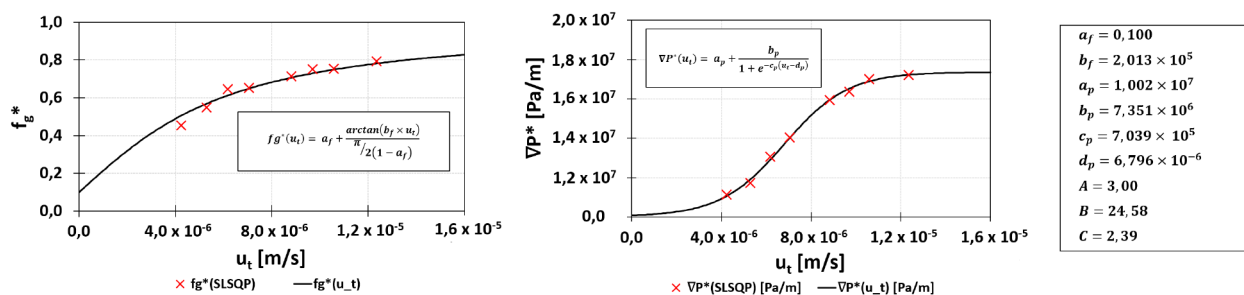

Figure 6. $\nabla P = f(f_g)$ curves fit to the Alvarez et al.[9] experimental data. Red crosses represent experimental points and were determined using $u_g = f(u_w)$ curves with pressure contours. Black curves are obtained through parameter functions of u_t and the optimization schema presented in Figure S2 in the Supporting Information. We set *epdry* = 10^4 for all u_t values.

of f_g. It outlines, as in the Alvarez et al.[9] experiments, that the curves at low quality, below f_g^*, are not linear. However, here, due to the small number of experimental data at low f_g, the fit may be rather approximate.

Concerning the evolution of the parameters with u_t (see Figure 9), the parametric equations again fit quite well the experimental points. As said above, the f_g^* value slightly increases but then rapidly remains stable. The pressure gradient also increases with a behavior closer to the one observed by Alavrez et al.[9] and seems to tend to a plateau.

Modified F_{shear} Subfunction within the STARS Foam Model. In the Foam Model section, two shear effects were cited: one for the variation of THE ∇P^* value with u_t and one for the foam quality variation within the low quality regime. To our knowledge, we first gather these two effects: the variation of ∇P^* is provided by linking the model parameter values with u_t and the shear effect in the low quality region is embedded by the F_{shear} function (equivalent to F_{cap}).

One significant contribution is the new definition of the F_{shear} function that is here linked to the Ostwald law and thus gainS physical meaning. Indeed this modifies the formula and

Figure 7. Parameters f_g^* and ∇P^* coming from the optimization process plotted against u_t with their dedicated curve fits and expressions. Red crosses come from the optimization process, and straight black lines represent fitted $f_g^*(u_t)$ and $\nabla P^*(u_t)$ subfunctions. Parameters A, B, and C from the F_{shear} function are also given. This figure gathers all information needed to cover all foam injection cases within the range of u_t studied.
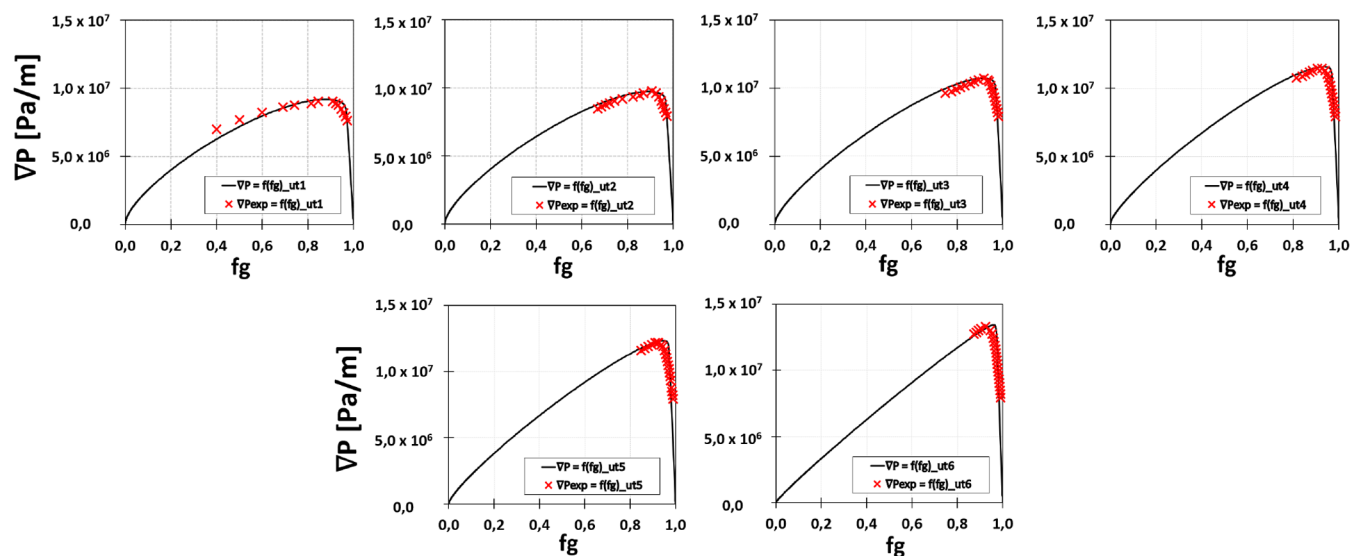
Figure 8. $\nabla P = f(f_g)$ curves fit to the Osterloh et al.[10] experimental data. Red crosses represent experimental points and were determined using $u_g = f(u_w)$ curves with pressure contours. Black curves are obtained through parameter functions of u_t and the optimization schema presented in Figure S2 in the Supporting Information. We set $epdry = 2 \times 10^4$ for all u_t values.
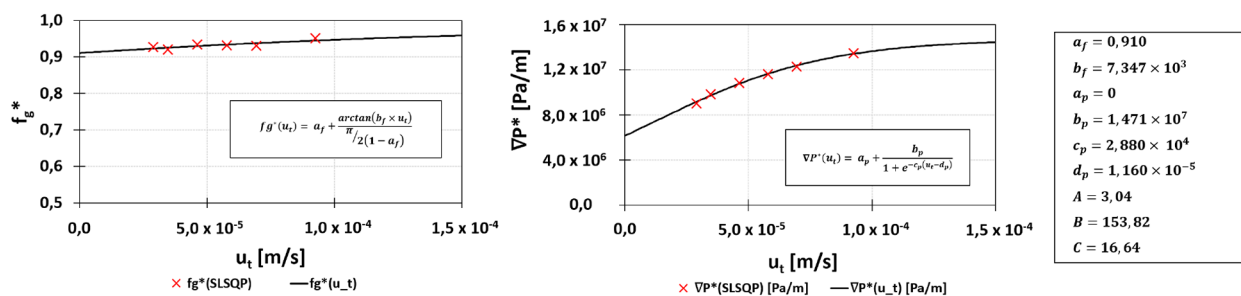

Figure 9. Parameters f_g^* and ∇P^* coming from the optimization process plotted against u_t with their dedicated curve fits and expressions. Red crosses come from the optimization process, and straight black lines represent fitted $f_g^*(u_t)$ and $\nabla P^*(u_t)$ subfunctions. Parameters A, B, and C from the F_{shear} function are also given. This figure gathers all the information needed to cover all foam injection cases within the range of u_t studied.

leads to a value of F_{shear} higher than one, but this is compensated by fitting the other parameters valid for the whole range of u_t values. However, the low quality shear behavior is also dependent on the u_t value as shown in Figure 1.

Our results show that a typical shear thinning occurs with u_t variation. This effect is evidenced at the transition point. Moreover, in the low quality regime another shear effect is present: at $f_g = 0.5$ the pressure gradient is higher than the average of $f_g = 0$ and $f_g = 1$ (i.e., Newtonian behavior);

therefore, the foam quality effect is a shear thickening below f_g^*. The Ostwald law parameters show that the intensity of this effect is also dependent on u_t.

Radial Effect on the Total Superficial Velocity and u_t Functions. All experiments demonstrated the need to consider the total superficial velocity effect on the foam behavior. Indeed, foam is always injected around a well bore, which leads to a rapid decrease of the total superficial velocity with the distance from the injection point. Interestingly, the variation of the pressure gradient with velocity is more
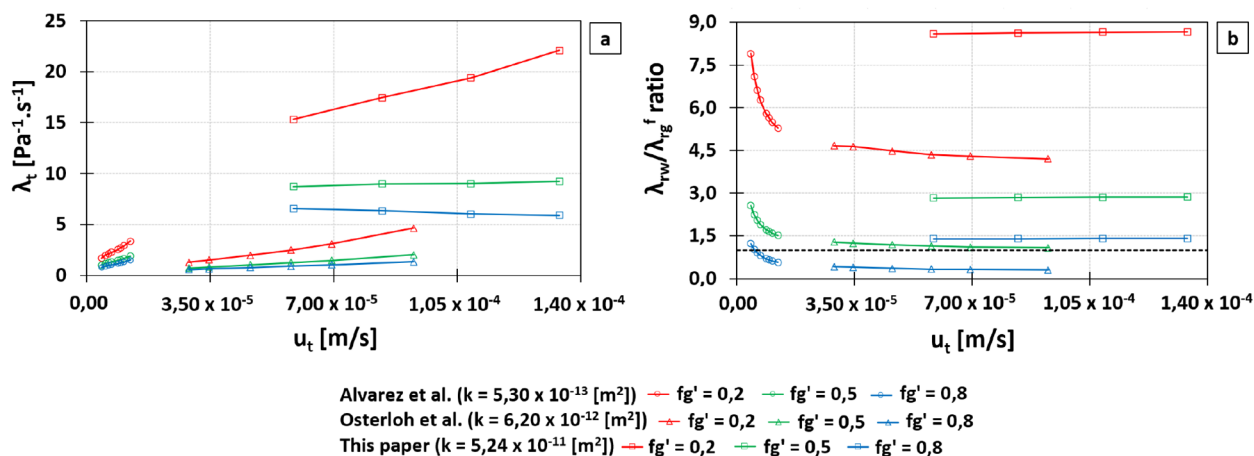
Figure 10. (a) Total mobility λ_t plotted against u_t for all experiments studied in this paper. Plots were done for three fg' values within the low quality regime. Permeability values are also given for the three studied cases. (b) Mobility ratios $\lambda_{rw}/\lambda_{rg}^f$ plotted against u_t for all experiments studied in this paper. Plots were done for three fg' values within the low quality regime. The dotted black line corresponds to the value $\lambda_{rw}/\lambda_{rg}^f = 1$ when both mobilities are equal.
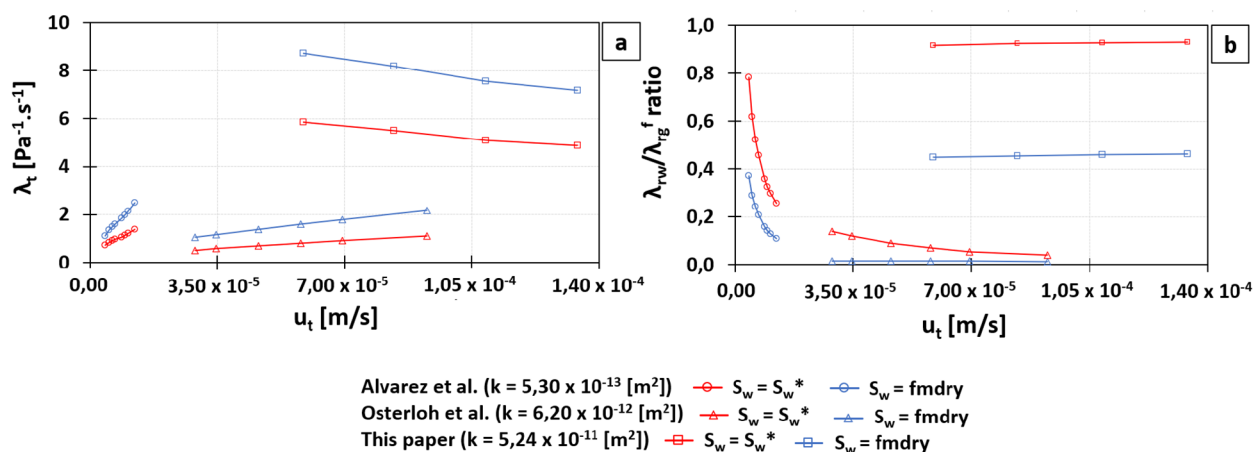
Figure 11. (a) Total mobility λ_t plotted against u_t for all experiments studied in this paper. Plots were done for $S_w = S_w^*$ and $S_w = fmdry$. Permeability values are also given for the three studied cases. (b) Mobility ratios $\lambda_{rw}/\lambda_{rg}^f$ plotted against u_t for all experiments studied in this paper. Plots were done for $S_w = S_w^*$ and $S_w = fmdry$.

pronounced in the presence of environmentally friendly surfactants (our experiments). This may suggest that the foam strength will decrease with distance from the well and the radius of action of the foam may be smaller than expected from lab experiments. Lee et al.[22] introduced the fact that the relative reduction in mobility generated by the presence of foam may depend on the permeability medium. In order to analyze this effect, the variations of the total mobility for the different experiments are illustrated in Figure 10.

In order to understand the origin of the total mobility variations, the equations of the phase mobilities must be detailed. Indeed, even though foam is composed of two phases (liquid and gas), in the proposed model of the original STARS one reproduces the steady state foam behavior only through the modification of the gas phase equation. The following two equation system use the generalized Darcy approach:

$$\begin{cases} u_g = u_t f_g = -\lambda_{rg}^f k\nabla P \\ u_w = u_t(1 - f_g) = -\lambda_{rw} k\nabla P \end{cases} \tag{20}$$

with u_g and u_w as the gas and liquid superficial velocities and $\lambda_{rg}^f = \dfrac{k_{rg}FM}{\mu_g}$ and $\lambda_{rw} = \dfrac{k_{rw}}{\mu_g}$ their mobilities, respectively. The total velocity is given by

$$u_t = -(\lambda_g^f + \lambda_w)k\nabla P \tag{21}$$

It appears from eq 21 that both fluid mobilities are implied to express ∇P vs u_t with foam. Remember here that F_{dry} is equal to one or closer within the low quality regime; thus, FM is only influenced by the F_{shear} subfunction. At first, as it is the objective of foam injection, Figure 10a shows that increasing the foam quality within the low quality regime reduces the total mobility λ_t. Second, it appears that the total mobility is influenced by u_t for all foam qualities in the Alvarez et al. experiments, i.e., at low velocities and permeability like in a deep reservoir. However, for the Osterloh et al. data and our experiments, this effect exists only at very low quality and is not supposed to be used in a field injection. Thus, curiously, in high permeability media, although the foam parameters are influenced by u_t, the total mobility in this regime is constant for
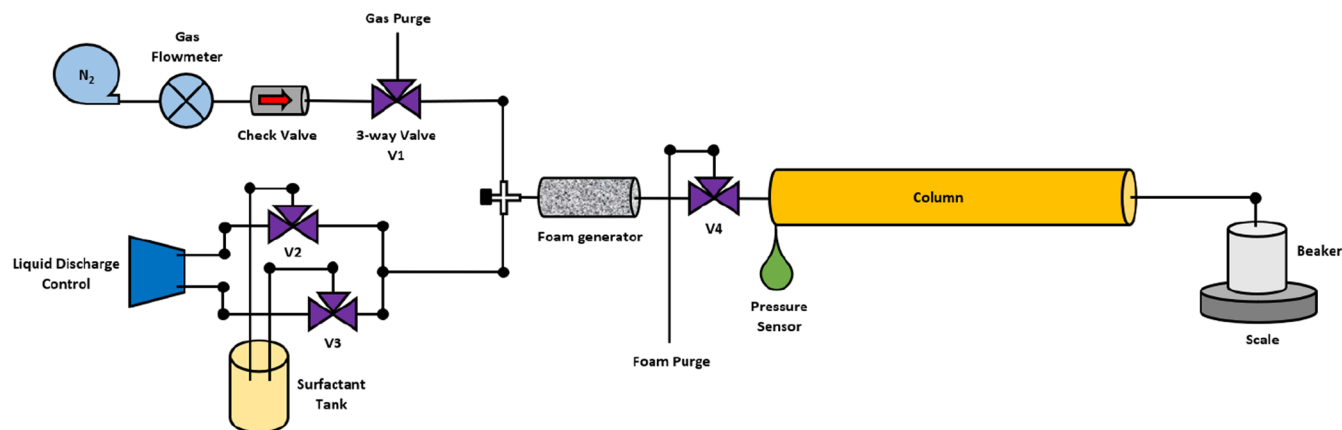
Figure 12. Schematic of the experimental apparatus.

one f_g value. This may arise from the fact that at f_g lower than f_g^* the role of water becomes prevalent.

The role of the mobilities of each phase is shown in Figure 10b, which presents the ratio of the water to the gas mobilities for the same conditions as previously. Again the Alvarez et al. experiments show different behavior than the others, with a ratio rapidly decreasing with velocity, while the other experiments show almost no u_t dependence. Moreover, for almost all experiments the ratio is above 1, showing, as we outlined above, that the role of water in the total mobility is the most important. So, in this regime, the mobility being linked to water behavior is not dependent on the total velocity.

In addition, we present in Figure 11a,b similar plots using the transition point and the $S_w = fmdry$ point to have a view on the high quality regime. Even if the high quality regime was not as detailed as the low quality regime, the fit in this area is still good. Figure 11a shows an increase of λ_t from S_w^* to $fmdry$ as expected. Our experimental results show a decrease of the total mobility with u_t when the two others from the literature present an increase. We can notice here that this increase is more pronounced for the Alvarez et al. experiments, which have the lowest permeability. The mobility ratios (Figure 11b) are constant against u_t in our experiments and decrease with f_g within the high quality regime for the other experiments.

CONCLUSION

In summary, we propose an approach to obtain the parameters of a modified STARS foam model type in an in situ environmental remediation context with a radial effect. This modified model presented here takes under consideration both the role of the foam quality and u_t on foam behavior by using an Ostwald−de Waele derived law as an F_{shear} subfunction. This new approach, applied to various u_t values and quality scans, demonstrates its ability to reproduce foam behaviors. Instead of using only one point to make the u_t dependence (often the f_g^* one) as shown in the literature, we proposed here to cover all the low quality regime of each quality scan to enhance the model. This model provides an accurate scan of all studied cases in this paper following each $\nabla P = f(f_g)$ shapes in both quality regimes. Moreover, a semiautomated process was set to estimate parameters of u_t functions using experimental data of multiple and dissimilar cases. In order to have an accurate fit, a certain amount of data is needed, especially in the low quality regime, to capture precisely the foam behavior. We also showed that the same mathematical formulation of the relationships between the model parameters and u_t can be used for each experimental set whatever the studied case, only modifying the values of the subparameters. The subparameter values seem to depend on both the medium and the surfactant, with no simple relationship with these factors at present.

EXPERIMENTAL SECTION

Several new 1-D foam flooding experiments at various total superficial velocities u_t and foam qualities f_g were carried out to complement previous experiments through the literature.[9,10]

Material and Methods. All the experiments were carried out in unconsolidated sand packs (MI 0.4/0.9 S_iO_2 99.1%). Sand packs had a diameter of 4.5 cm and a length of 27.7 cm. The permeability to water was calculated from a Darcy test for each column before flooding experiments. An average permeability of 5.24×10^{-11} m^2 with a standard deviation of 1.37×10^{-11} m^2 was obtained for the 5 columns. Saponin, which is naturally derived from plants, was used as a nonionic, biodegradable, and renewable surfactant in a environmental burden reduction context.[23] Tap water was used as the liquid phase, and the critical micelle concentration of the saponin (CMC) was previously determined through the pending water drop test[24] with a value of 0.062 wt %. Nitrogen (N_2) was used as the gas phase during the experiments.

Experimental Setup. A schematic of the apparatus is presented in Figure 12. The same column was used for each experiment (sand was replaced in it) and placed in a horizontal position with injection from the left. A pressure tap was located next to the injection point within the porous medium, and the pressure was recorded by an Idroscan AEP transducer with a range of 0−5 bar and a resolution of 1 mbar. A foam generator was used in order to improve the gas and liquid mixture before the entry into the porous medium. This component has an internal diameter of 3.4 cm and a length of 12.5 cm and was filled by 2 mm glass beads.

The liquid and gas were coinjected at defined proportions before entering the foam generator. The gas injection was controlled by a Bronkhorst gas thermal mass flow meter with a range of 0.4−20 mL/min. The liquid discharge control was performed by a dual syringe injector (60 mL volume) linked to a stepper motor. This device avoids syringe reloading and, thus, injection discontinuity by a simultaneous charge and discharge of syringes. A beaker was used to collect the effluent, and a scale was used to check the liquid flow equality between inlet and outlet. This equality coupled to the stabilization of

the pressure value indicates that the steady state regime was reached.

Experimental Procedures. All experiments were carried out at room temperature (20 °C) with an atmospheric outlet pressure. Each column was filled with sand and tap water following the same procedure, which consists of alternated small additions of water and sand interspersed with tamp operations. The porosity was deduced from the total water volume added to fill the column and its dimensions.

The foam generator was placed vertically (inlet downward), and tap water was injected with the foam purge active (see 3-way valve V4, Figure 12) to release the air, and then the foam generator was placed horizontally, after which the foam purge was closed and the column was connected to the apparatus keeping the water flow to avoid air bubbles into pipes. Then, a Darcy test was done to estimate the water permeability of the sample.

After this step, the column and the foam generator were filled with surfactant solution at 10 CMC at one pore volume to prevent adsorption of the surfactant by the porous media during foam injection. The liquid discharge control and the gas flow meter were set to the desired flow value, using the gas purge. As soon as the gas flow was stabilized, the gas purge was closed to start foam injection into the foam generator, keeping the foam purge activated. When the steady state was reached into the foam generator, the foam injection started in the column for a minimum of 3 VP of both fluids.

We assume that the steady state is reached when the pressure drop held constant over time. The bubbles dynamic (creation, deformation, and destruction) leads to pressure oscillations even in the steady state. The outlet liquid flow rate was compared to the inlet one, and their equality helped to confirm that steady state was reached. The same column was used for a new injection at the same foam quality with a lower total superficial velocity. When the effluent of the foam purge was stabilized, the next flooding experiment was started by switching it.

At least 20 flooding experiments were done combining different total superficial velocities and foam qualities. Table 1 summarizes the experimental conditions of each test and their average pressure gradient responses once steady state has been reached.

ASSOCIATED CONTENT

ⓢ Supporting Information

The Supporting Information is available free of charge at https://pubs.acs.org/doi/10.1021/acsomega.1c04899.

Figure S1 presents the F_{shear} subfunction used to cover the low quality regime by modifying the *fmmob* value, and Figure S2 presents the detailed flowchart of the fitting method presented is this paper (PDF)

AUTHOR INFORMATION

Corresponding Authors

Alexandre Vicard − ENSEGID - EA 4592 Georessources et Environnement, Institut Carnot Isifor, 33607 Pessac, France; Consortium innovaSol, https://www.innovasol.org/; ⓞ orcid.org/0000-0003-0005-7253; Email: alexandre.vicard@gmail.com

Olivier Atteia − ENSEGID - EA 4592 Georessources et Environnement, Institut Carnot Isifor, 33607 Pessac, France; Consortium innovaSol, https://www.innovasol.org/; Email: olivier.atteia@ensegid.fr

Authors

Henri Bertin − I2M, UMR CNRS 5295, Université de Bordeaux, Talence Cedex 33405, France

Jean Lachaud − I2M, UMR CNRS 5295, Université de Bordeaux, Talence Cedex 33405, France

Complete contact information is available at:
https://pubs.acs.org/10.1021/acsomega.1c04899

Notes

The authors declare no competing financial interest.

■ NOMENCLATURE

λ_{rg}^f	Relative mobility of the gas phase in the presence of foam $(Pa \cdot s)^{-1}$
λ_t	Total mobility $(Pa \cdot s)^{-1}$
λ_{rg}	Relative mobility of the gas phase $(Pa \cdot s)^{-1}$
λ_{rw}	Mobility of the water $(Pa \cdot s)^{-1}$
μ_g	Dynamic viscosity of the gas phase $(Pa \cdot s)$
μ_w	Dynamic viscosity of the water $(Pa \cdot s)$
μ_{app}^f	Apparent viscosity of the foam $(Pa \cdot s)$
∇P	Pressure gradient $(Pa \cdot m^{-1})$
ρ_g	Density of the gas phase $(kg \cdot m^{-3})$
epcap	Parameter that captures shear thinning behavior in the low quality regime
epdry	Parameter that controls the abruptness of foam collapse
f_g	Foam quality
f_g^p	Normalized position within the low quality regime
f_g^*	Foam quality at the transition point
F_i	additional factors from the STARS (CMG) model
fcap	The smallest capillary number expected to be encountered
FM	Mobility factor from the STARS (CMG) model
fmdry	Critical water saturation value at which foam starts to collapse
fmmob	Reference gas-mobility-reduction factor for wet foams
g	Gravitational force $(m \cdot s^{-2})$
k	Permeability (m^2)
k_{rg}	Relative permeability of the gas phase
k_{rg}^0	Brooks and Corey constant for the gas phase
k_{rw}	Relative permeability of the liquid phase
k_{rw}^0	Brooks and Corey constant for the water
n_g	Brooks and Corey gas phase exponent
n_w	Brooks and Corey water exponent
N_{Ca}	Capillary number
RF	Resistance factor
S_e	Effective water saturation
S_w	Water saturation
S_w^*	Critical water saturation value at which foam starts to collapse
$S_{g,r}$	Residual gas saturation
$S_{w,r}$	Residual water saturation
u_g	Superficial velocity of the gas phase $(m \cdot s^{-1})/(m \cdot d^{-1})$
u_t	Total superficial velocity $(m \cdot s^{-1})/(m \cdot d^{-1})$
u_w	Superficial velocity of the water $(m \cdot s^{-1})/(m \cdot d^{-1})$

■ REFERENCES

(1) Eftekhari, A. A.; Krastev, R.; Farajzadeh, R. Foam stabilized by fly ash nanoparticles for enhancing oil recovery. *Ind. Eng. Chem. Res.* **2015**, *54*, 12482−12491.

(2) Farajzadeh, R.; Wassing, B.; Boerrigter, P. *Foam assisted gas oil gravity drainage in naturally-fractured reservoirs*; SPE Annual Technical Conference and Exhibition, 2010.

(3) Chabert, M.; Morvan, M.; Nabzar, L. *Advanced screening technologies for the selection of dense CO2 foaming surfactants*; SPE Improved Oil Recovery Symposium, 2012.

(4) Maire, J.; Fatin-Rouge, N. Surfactant foam flushing for in situ removal of DNAPLs in shallow soils. *Journal of hazardous materials* **2017**, *321*, 247−255.

(5) Hirasaki, G.; Miller, C.; Szafranski, R.; Tanzil, D.; Lawson, J.; Meinardus, H.; Jin, M.; Londergan, J.; Jackson, R.; Pope, G.; Wade, W. *Field demonstration of the surfactant/foam process for aquifer remediation*; SPE Annual Technical Conference and Exhibition, 1997.

(6) Portois, C.; Essouayed, E.; Annable, M. D.; Guiserix, N.; Joubert, A.; Atteia, O. Field demonstration of foam injection to confine a chlorinated solvent source zone. *Journal of contaminant hydrology* **2018**, *214*, 16−23.

(7) Kovscek, A. R.; Radke, C. J. *Fundamentals of foam transport in porous media*; 1993; DOI: 10.2172/10192736

(8) Rossen, W. R. A critical review of Roof snap-off as a mechanism of steady-state foam generation in homogeneous porous media. *Colloids Surf., A* **2003**, *225*, 1−24.

(9) Alvarez, J.; Rivas, H.; Rossen, W. Unified model for steady-state foam behavior at high and low foam qualities. *SPE journal* **2001**, *6*, 325−333.

(10) Osterloh, W.; Jante, M. *Effects of gas and liquid velocity on steady-state foam flow at high temperature*; SPE/DOE Enhanced Oil Recovery Symposium, 1992.

(11) Khatib, Z.; Hirasaki, G.; Falls, A. Effects of capillary pressure on coalescence and phase mobilities in foams flowing through porous media. *SPE reservoir engineering* **1988**, *3*, 919−926.

(12) Brooks, R. H.; Corey, A. T. Properties of porous media affecting fluid flow. *Journal of the irrigation and drainage division* **1966**, *92*, 61−88.

(13) Van Genuchten, M. T. A closed-form equation for predicting the hydraulic conductivity of unsaturated soils. *Soil science society of America journal* **1980**, *44*, 892−898.

(14) Boeije, C. S.; Rossen, W. Fitting foam-simulation-model parameters to data: I. coinjection of gas and liquid. *SPE Reservoir Evaluation & Engineering* **2015**, *18*, 264−272.

(15) Cheng, L.; Reme, A.; Shan, D.; Coombe, D.; Rossen, W. *Simulating foam processes at high and low foam qualities*; SPE/DOE improved oil recovery symposium, 2000.

(16) Ma, K.; Lopez-Salinas, J. L.; Puerto, M. C.; Miller, C. A.; Biswal, S. L.; Hirasaki, G. J. Estimation of parameters for the simulation of foam flow through porous media. Part 1: the dry-out effect. *Energy Fuels* **2013**, *27*, 2363−2375.

(17) Lee, W.; Lee, S.; Izadi, M.; Kam, S. I. Dimensionality-dependent foam rheological properties: how to go from linear to radial geometry for foam modeling and simulation. *SPE Journal* **2016**, *21*, 1669−1687.

(18) Farajzadeh, R.; Lotfollahi, M.; Eftekhari, A.; Rossen, W.; Hirasaki, G. Effect of permeability on implicit-texture foam model parameters and the limiting capillary pressure. *Energy Fuels* **2015**, *29*, 3011−3018.

(19) Zeng, Y.; Muthuswamy, A.; Ma, K.; Wang, L.; Farajzadeh, R.; Puerto, M.; Vincent-Bonnieu, S.; Eftekhari, A. A.; Wang, Y.; Da, C.; Joyce, J. C.; Biswal, S. L.; Hirasaki, G. J. Insights on foam transport from a texture-implicit local-equilibrium model with an improved parameter estimation algorithm. *Ind. Eng. Chem. Res.* **2016**, *55*, 7819−7829.

(20) Abbaszadeh, M.; Nia Korrani, A. K.; Lopez-Salinas, J. L.; Rodriguez-de La Garza, F.; Villavicencio Pino, A.; Hirasaki, G. *Experimentally-based empirical foam modeling*; SPE Improved Oil Recovery Symposium, 2014.

(21) Ding, L.; Cui, L.; Jouenne, S.; Gharbi, O.; Pal, M.; Bertin, H.; Rahman, M. A.; Romero, C.; Guérillot, D. Estimation of Local Equilibrium Model Parameters for Simulation of the Laboratory Foam-Enhanced Oil Recovery Process Using a Commercial Reservoir Simulator. *ACS omega* **2020**, *5*, 23437−23449.

(22) Lee, H. O.; Heller, J. P. Laboratory measurements of CO2-foam mobility. *SPE Reservoir Engineering* **1990**, *5*, 193−197.

(23) Schmitt, C.; Grassl, B.; Lespes, G.; Desbrières, J.; Pellerin, V.; Reynaud, S.; Gigault, J.; Hackley, V. Saponins: A renewable and biodegradable surfactant from its microwave-assisted extraction to the synthesis of monodisperse lattices. *Biomacromolecules* **2014**, *15*, 856−862.

(24) Forey, N.; Atteia, O.; Omari, A.; Bertin, H. Saponin foam for soil remediation: On the use of polymer or solid particles to enhance foam resistance against oil. *Journal of contaminant hydrology* **2020**, *228*, 103560.